Engineering Computations

On the modeling of oil well drilling processes

Esteban Della Nave Eduardo Natalio Dvorkin

On the modeling of oil well drilling processes

Esteban Della Nave and Eduardo Natalio Dvorkin
SIM&TEC S.A., Buenos Aires, Argentina

Received 19 March 2013
Revised 25 March 2014
22 May 2014
Accepted 29 May 2014

Abstract

Purpose – The purpose of this paper is to present the development of a simulator of oil well drilling processes.

Design/methodology/approach – The simulator incorporates the main variables that are used by drilling engineers in the definition of the drilling processes. The code is useful a priori, in the design of a drilling process, as a tool for comparing different design options and predicting their results and a posteriori of a failure to understand its genesis and therefore provide know-why to improve the drilling techniques.

Findings – The developed finite element simulator uses a co-rotational Bernoulli beam element, an explicit time integration scheme and an explicit contact algorithm. The numerical results show that the simulator is stable and provides consistent solutions.

Practical implications – During the drilling of oil wells, the fatigue damage and wear of the drilling column is of utmost concern. To determine the mechanical behavior of the drilling column standard simplified analyses are usually performed using commercially available codes; however, those standard analyses do not include a transient dynamic simulation of the process; hence, it is necessary to develop a specific tool for the detailed dynamic simulation of drilling processes.

Originality/value – A simulator able to perform a description of the drilling process in the time range will be an important contribution to the tools used by drilling engineers.

Keywords Simulation, Finite elements, Oil drilling

Paper type Research paper

1. Introduction

The drilling of oil wells is an involved process in which a well of prescribed trajectory is accurately constructed trough several thousand meters of different rock formations (see Figures 1 and 2).

During the drilling of oil wells, the fatigue damage and wear of the drilling column is of utmost concern (Shathuvalli *et al.*, 2005; Sikal *et al.*, 2008); especially when using the casing while drilling technique (CWD) in which the well is simultaneously drilled and cased (Warren *et al.*, 2000). In this process the drilling column, instead of being composed by heavy drill pipes is composed by the much lighter casing pipes; hence, the wear and fatigue effects are more relevant. To determine the mechanical behavior of the drilling column standard simplified analyses (Rae *et al.*, 2005) are usually performed using commercially available codes; however, those standard analyzes do not include a transient dynamic simulation of the process; hence, it is necessary to develop a specific tool for the detailed dynamic simulation of drilling processes.

In this paper we describe the fundamentals of the code that we developed for modeling drilling processes. It is important to remark that the model that we developed does not incorporate any ad hoc simplification (e.g. "stiff strinf" or "soft string" models), therefore, the model results are not biased by assumptions that may neglect certain effects.

In the second section of this paper we discuss the finite element formulation that we implemented in the drilling simulator. In the third section we discuss the simulation

The authors gratefully acknowledge the support of TENARIS.

Engineering Computations: International Journal for Computer-Aided Engineering and Software
Vol. 32 No. 2, 2015
pp. 387-405

0264-4401
DOI 10.1108/EC-03-2013-0093

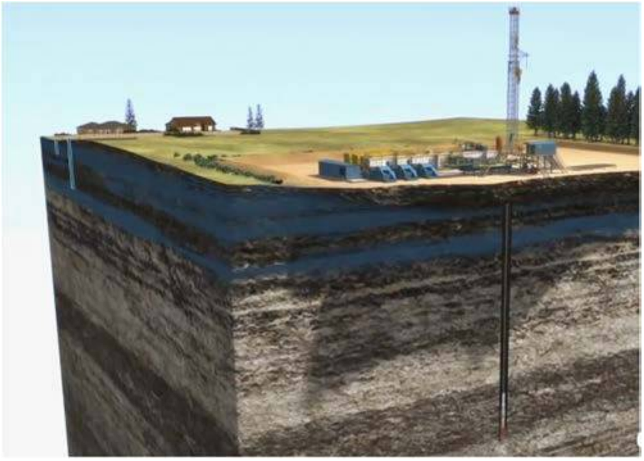

Figure 1.
Scheme of the drilling of a vertical oil well

Figure 2.
Drilling of a curved directional well

set-up; that is to say, the main assumptions used to model the drilling processes, the required data input and the imposed boundary conditions. In the fourth section we present some illustrative numerical examples and discuss the requirements for getting stable solutions. In Appendix we describe the geometrical representation of the well trajectory usually used by drilling engineers. Our simulator pre-processor includes a module for translating the input geometrical data into Cartesian coordinates.

The need for geometrical nonlinear analysis

It is well known that axial compressive load acting on a tubular column diminishes its lateral stiffness while an axial tensile load increases its lateral stiffness. This is a geometrical nonlinear effect and can only be modeled considering the equilibrium of the column in its deformed configuration (Bathe, 1996; Dvorkin and Goldschmit, 2005).

In a static analyses, in the lower compressed sector of the drilling column, the diminishing of the lateral stiffness can lead to the buckling of the column, which is a contained buckling, due to the lateral restraint imposed by the oil well (Lubinski and Althouse, 1962; Mitchell, 2003).

In some drilling operations the pressure of the mud inside the column (internal pressure when referring to the column) is higher than the pressure in the annulus between the well and the column (external pressure when referring to the column); when considering the buckling of the column, the internal pressure has a destabilizing effect; that is to say, it lowers the axial buckling critical load. On the contrary the external pressure has a stabilizing effect; that is to say, it increases the axial buckling critical load. These effects were discussed in Palmer and Martin (1975) and Dvorkin and Toscano (2001). In this paper we will consider that the internal and external pressures are balanced.

In a dynamic analysis the effect of the axial load on the lateral stiffness is evidenced analyzing the drilling column natural frequencies; a tensile load increases the transversal bending natural frequencies while a compressive load decreases them. Since it is necessary to incorporate these axial load effects to the model, we developed our code using a geometrically nonlinear formulation limited to the case of small strains which closely represents the actual operation conditions.

2. The finite element formulation

In the simulator that we developed, the pipes column is modeled using beam elements and it incorporates the following features:

- co-rotational beam elements used to model the pipes column;
- lumped mass matrix;
- frictional contact algorithm used to model the interaction between the pipes and the well;
- fluid damping introduced by the fluids inside the well; and
- explicit time integration algorithm.

2.1 The beam element formulation

The beam element that we implemented is the standard Bernoulli beam element with a tubular cross section; hence, we neglect the effect of shear deformations (Bathe and Bolourchi, 1979).

We implemented a co-rotational formulation aimed at the modeling of large displacements/rotations but infinitesimal strains, which is the case in the modeling of drilling operations.

For a two-node element "e" we define:

${}^{0}x_i^k\,(k = 1-2)\,(i = 1-3)$: i-coordinate of the k-node at time $t = 0$ (reference configuration);

${}^{t}u_i^k\,(k = 1-2)\,(i = 1-3)$: i-displacement of the k-node at the t-configuration;

${}^{t}\theta_i^k\,(k = 1-2)\,(i = 1-3)$: i-rotation of the k-node at the t-configuration;

For the "e" element we define the axial vector:

$$ {}^{0}\underline{V}_r^{(e)} = \frac{{}^{0}x_i^2 - {}^{0}x_i^1}{\sum_j \left({}^{0}x_j^2 - {}^{0}x_j^1 \right)} \underline{e}_i \tag{1} $$

and we introduce two arbitrary vectors $\left({}^{0}\underline{V}_s^{(e)}, {}^{0}\underline{V}_t^{(e)} \right)$ that form with ${}^{0}\underline{V}_r^{(e)}$ an ortho-normal set.

At the *t*-configuration we calculate the new axial vector:

$$\frac{{}^{t}\underline{V}_{r}^{(e)} = {}^{t}x_{i}^{2} + {}^{t}u_{i}^{2} - {}^{t}x_{i}^{1} - {}^{t}u_{i}^{1}}{\sqrt{\sum_{j}\left({}^{t}x_{j}^{2} + {}^{t}u_{j}^{2} - {}^{t}x_{j}^{1} - {}^{t}u_{j}^{1}\right)^{2}}\, e_{i}} \tag{2}$$

The angle between ${}^{0}\underline{V}_{r}^{(e)}$ and ${}^{t}\underline{V}_{r}^{(e)}$ is:

$${}^{t}\alpha^{(e)} = \cos^{-1}\left({}^{0}\underline{V}_{r}^{(e)} \cdot {}^{t}\underline{V}_{r}^{(e)}\right) \tag{3}$$

We now define the rotation vector:

$${}^{t}\underline{\Theta}^{(e)} = {}^{t}\alpha^{(e)} \frac{{}^{0}\underline{V}_{r}^{(e)} \times {}^{t}\underline{V}_{r}^{(e)}}{\left\| {}^{0}\underline{V}_{r}^{(e)} \times {}^{t}\underline{V}_{r}^{(e)} \right\|} = {}^{t}\Theta_{i}\underline{e}_{i}; \tag{4}$$

and the corresponding rigid rotation matrix (Dvorkin *et al.*, 1988):

$${}^{t}\underline{R}^{(e)} = \underline{I} + \frac{\sin {}^{t}\alpha^{(e)}}{{}^{t}\alpha^{(e)}} \begin{bmatrix} 0 & -{}^{t}\Theta_{3} & {}^{t}\Theta_{2} \\ {}^{t}\Theta_{3} & 0 & -{}^{t}\Theta_{1} \\ -{}^{t}\Theta_{2} & {}^{t}\Theta_{1} & 0 \end{bmatrix}$$

$$+\frac{1}{2}\left[\frac{\sin\left(\frac{{}^{t}\alpha^{(e)}}{2}\right)}{\left(\frac{{}^{t}\alpha^{(e)}}{2}\right)}\right]^{2} \begin{bmatrix} 0 & -{}^{t}\Theta_{3} & {}^{t}\Theta_{2} \\ {}^{t}\Theta_{3} & 0 & -{}^{t}\Theta_{1} \\ -{}^{t}\Theta_{2} & {}^{t}\Theta_{1} & 0 \end{bmatrix} \begin{bmatrix} 0 & -{}^{t}\Theta_{3} & {}^{t}\Theta_{2} \\ {}^{t}\Theta_{3} & 0 & -{}^{t}\Theta_{1} \\ -{}^{t}\Theta_{2} & {}^{t}\Theta_{1} & 0 \end{bmatrix}. \tag{5}$$

Using the above defined rotation matrix we write:

$$\begin{aligned} {}^{t}\underline{V}_{s}^{(e)} &= {}^{t}\underline{R}_{(e)} \cdot {}^{0}\underline{V}_{s}^{(e)} \\ {}^{t}\underline{V}_{t}^{(e)} &= {}^{t}\underline{R}_{(e)} \cdot {}^{0}\underline{V}_{t}^{(e)}. \end{aligned} \tag{6}$$

2.1.1 The beam element torsion. Along each element (*e*) the torsional angle has a linear distribution and at each node "*k*":

$${}^{t}\underline{\theta}_{torsion}^{k} = \left({}^{t}\underline{\theta}_{k} \cdot {}^{t}\underline{V}_{r}^{e}\right) {}^{t}\underline{V}_{r}^{e}. \tag{7}$$

2.1.2 The beam element bending. To get the bending displacements we subtract from the total displacements the ones corresponding to a rigid body motion, and to the torsional deformation:

$$\begin{aligned} {}^{t}\underline{u}_{bending}^{1} &= 0 \\ {}^{t}\underline{\theta}_{bending}^{1} &= 0 \\ {}^{t}\underline{u}_{bending}^{2} &= {}^{t}\underline{u}_{2} - {}^{t}\underline{u}_{1} - \left[{}^{t}R^{(e)} \cdot \left({}^{o}\underline{x}_{2} - {}^{o}\underline{x}_{1}\right) - \left({}^{o}\underline{x}_{2} - {}^{o}\underline{x}_{1}\right)\right] \\ {}^{t}\underline{\theta}_{bending}^{2} &= {}^{t}\underline{\theta}^{2} - {}^{t}\underline{\theta}^{1} - {}^{t}\underline{\theta}_{torsion}^{2}. \end{aligned} \tag{8}$$

2.1.3 The beam element stress resultants. In the system $\left({}^tV_r^{(e)}, {}^tV_s^{(e)}, {}^tV_t^{(e)}\right)$ located in the deformed configuration we determine:

- the axial stress resultants using the difference between ${}^t\underline{u}_2$ and ${}^t\underline{u}_1$ projected on ${}^t\underline{V}_r^{(e)}$;
- the torsional moment using the angle determined in Equation (7); and
- the bending moments and bending shears using the relative generalized bending displacements calculated with Equation (8).

2.1.4 The beam element mass matrix. We use a lumped mass matrix with concentrated displacement and rotational masses at the nodes.

2.2 The frictional contact algorithm

We implemented a frictional contact algorithm based on the explicit frictional predictive/corrective contact algorithm published by Cirak and West (2005).

In the model we introduce the following hypotheses:

- the contact column/well is localized at the boxes (couplings) of the inter-pipe connections (their OD is larger than the OD of the pipes, as shown in Figure 3); and
- in order to get a stable solution, avoiding "chattering", we only consider contact every "NC" boxes and at Δt_c time intervals (see Section 4 where we discuss the solution stability using the results of our numerical experimentation).

2.2.1 Algorithm predictive phase. In Figure 4 we schematize a well section (*i, i+1*) and a column section ($N-1$, N). In the figure the column interpenetrates the well and therefore the contact algorithm needs to restore the geometrical compatibility.

For the *N*-node of the column:

- *Localize the well section that contains the node*: if the node is in the *i-th* well section and the *x*-coordinate is the vertical coordinate, we know that $x_I^{well} < {}^tx_N < x_{I+1}^{well}$.
- *From the geometry in* Figure 4, we calculate the distance from a point located on the box OD to the well wall (*dist*).

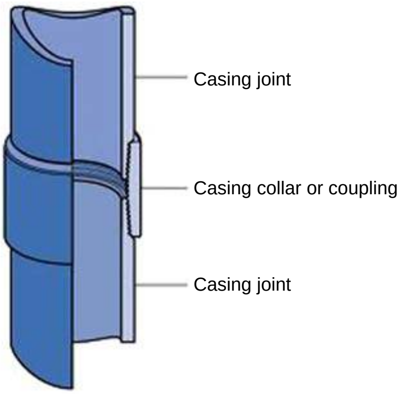

Figure 3. Connection box (coupling)

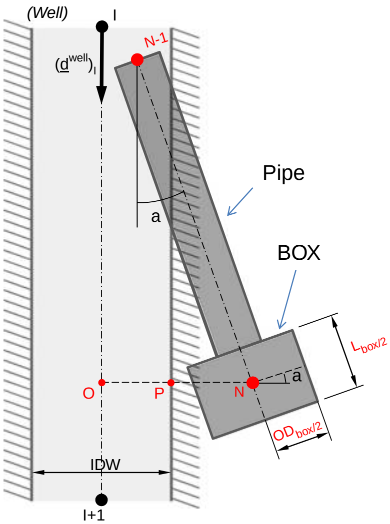

Figure 4.
Geometry of the contact pipe/well (in this case the contact algorithm needs to correct the geometry and the kinematics)

If *dist* > *(IDW/2)* (as drawn in Figure 4) the N-node of the column interpenetrates the well and the prediction results for this node will need to be corrected in the corrective step of the algorithm.

2.2.2 Algorithm contact corrections. When from the analysis of the contact geometry for the *N*-node of the column we get interference between the box and the well, we go through the following corrective steps:

- *Calculate* (see Figure 4):

$$ {}^{t}\underline{r}_O = \underline{r}_I + \left[\underline{d}_I^{well} \cdot \left({}^{t}\underline{r}_N - \underline{r}_i\right)\right] \underline{d}_I^{well} \tag{9} $$

- *Correct the position of the N-node of the column*: making zero the interference:

$$ {}^{t}\underline{r}_N^{new} = {}^{t}\underline{r}_O + \left(\frac{IDW}{2} - d2\right) \frac{\left({}^{t}\underline{r}_N - {}^{t}\underline{r}_O\right)}{\left\| {}^{t}\underline{r}_N - {}^{t}\underline{r}_O \right\|} \tag{10} $$

- *Velocity correction*: the algorithm that we implemented conserves the energy and momentum of each of the column nodes independently; hence, the solution has a dependence on the order that we use to loop over the column nodes. This error tends to zero when we decrease the time step.

We define the vector ${}^{t}\underline{r}_{ON} = \left({}^{t}\underline{r}_N^{new} - {}^{t}\underline{r}_O\right)$, the unit vector in the normal direction (*n-direction*) is ${}^{t}\underline{r}_{ON} / \left\| {}^{t}\underline{r}_{ON} \right\|$ and a unit vector in a tangential direction (*w-direction*) is ${}^{t}w = \underline{d}_I^{well} \times \left({}^{t}\underline{r}_{ON} / \left\| {}^{t}\underline{r}_{ON} \right\|\right)$.

The velocity of the N-node after solving the step $t \to t+\Delta t$ and before imposing the contact condition is ${}^{t+\Delta t}\underline{\widehat{v}}^N \left({}^{t+\Delta t}\widehat{v}_d^N,\ {}^{t+\Delta t}\widehat{v}_n^N;\ {}^{t+\Delta t}\widehat{v}_w^N \right)$. After the impact column/well the normal velocity component is corrected conserving energy and momentum to (Cirak and West, 2005):

$$ {}^{t+\Delta t}v_n^N = {}^{t+\Delta t}\widehat{v}_n^N + \frac{{}^{t+\Delta t}_{\ \ t}J_n^N}{m_N} \tag{11} $$

where:

$$ {}^{t+\Delta t}_{\ \ t}J_n^N = \frac{-2m_N\ {}^t\hat{v}_n^N - \sqrt{\left(2m_N\ {}^t\widehat{v}_n^N\right)^2 - 8m_N\left({}^t\underline{F}_N^{ext} - {}^t\underline{F}_N\right)\cdot\left({}^t\underline{r}_P - {}^t\underline{r}_N\right)}}{2} \tag{12} $$

In the above equation, ${}^t\underline{F}_N^{ext}$ and ${}^t\underline{F}_N^{int}$ are the external and internal forces on the N-node of the column.

- *Angular velocity correction:* the sliding impulse in the $[t, t+\Delta t]$ interval is:

$$ {}^{t+\Delta t}_{\ \ t}J_{sliding}^N = \min\left(m_n\, {}^{t+\Delta t}\widehat{v}_{sliding}^N;\ \mu\ {}^{t+\Delta t}_{\ \ t}J_n^N \right). \tag{13} $$

In the above equation, ${}^{t+\Delta t}\widehat{v}_{sliding}^N = \sqrt{\left({}^{t+\Delta t}\widehat{v}_d^N\right)^2 + \left({}^{t+\Delta t}\widehat{v}_w^N\right)^2}$ and μ is the column/well friction coefficient. The tangential velocity component is corrected to (Cirak and West, 2005):

$$ {}^{t+\Delta t}v_{sliding}^N = {}^{t+\Delta t}\widehat{v}_{sliding}^N - \frac{{}^{t+\Delta t}\widehat{v}_{sliding}^N}{\left\| {}^{t+\Delta t}\widehat{v}_{sliding}^N \right\|} \frac{{}^{t+\Delta t}_{\ \ t}J_{sliding}^N}{m_N} \tag{14} $$

For the angular velocity $\left({}^{t+\Delta t}\underline{\Omega}\right)$ the correction we use:

$$ {}^{t+\Delta t}(\Omega)_i^N = {}^{t+\Delta t}\widehat{(\Omega)}_i^N - \frac{{}^{t+\Delta t}\widehat{v}_i^N}{\left\| {}^{t+\Delta t}\widehat{\underline{v}}_N \right\|} \frac{{}^{t+\Delta t}_{\ \ t}J_{sliding}^N}{I_{ii}} \left(\frac{OD}{2} \right); \tag{15} $$

where $(i = 1,2,3)$ and I_{ii} is the rotational inertia moment of the section with respect to the ii-axis.

2.2.3 Frictional effects: numerical experimentation. To illustrate on the effect of the friction coefficient value, in Figure 5 we schematize the drilling column movement for different values of this coefficient. From that figure we see that when the friction coefficient increases its value the movement of the column changes and the contact area column-well shrinks and the wear of the pipes gets localized along a generatrix of the column.

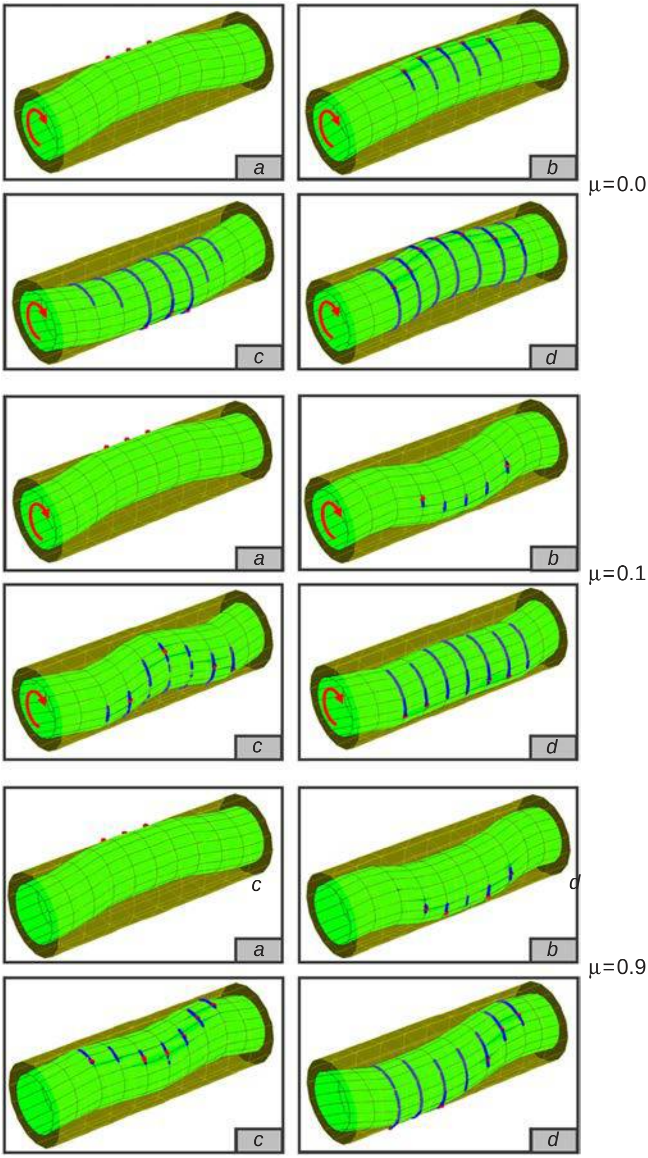

Notes: In blue we show the time evolution of the contact points and in red the location of the contact point at the time of the drawn configuration. It is indicated with "a,b,c and d" four consecutive configurations

Figure 5.
Effect of the friction coefficient column/well

2.3 Fluid damping

In this subsection we analyze the modeling of the damping effects introduced by the fluids inside the well.

2.3.1 Damping in the axial direction. When the column is moving with an axial velocity, the shear stress opposing the movement is:

$$^{t}\tau = \frac{2\mu_{fluid}\ {}^{t}v_{axial}}{(IDW - od)} \tag{16}$$

where μ_{fluid} is the external fluid kinematic viscosity, $^{t}v_{axial}$ is the linear velocity along the element axis and od is the pipes outside diameter.

The force opposed to the axial movement at node N is modeled as:

$$^{t}F^{N}_{axial} = {}^{t}\tau\pi(od)l \tag{17}$$

where l is the distance between the center of the elements above and beneath the N-node.

2.3.2 Damping in the radial direction. The drag force opposing the velocity in the radial direction is modeled as:

$$^{t}F_{radial} = \frac{1}{2}\delta_{fluid}A\,{}^{t}C_D\left({}^{t}v_{rad}\right)^2 \tag{18}$$

where $^{t}C_D$ is the drag coefficient for a cylinder with a fluid of a density δ_{fluid} moving towards it with a velocity $^{t}v_{rad}$.

2.3.3 Damping for the rotational movement. The damping moment opposing the rotational movement is modeled as:

$$^{t}M = 0.5\mu_{fluid}(od)^3 l\,{}^{t}\omega\frac{\pi}{(IDW - od)} \tag{19}$$

In the above equation, for each element, ω is the angular velocity along the element axis.

2.3.4 Fluid damping: numerical experimentation. In Figure 6 we show an example of the effect of the damping on torsional vibrations and in Figure 7 we show an example of the effect of damping on axial vibrations.

2.4 The time integration algorithm

During an incremental analysis we solve the nonlinear dynamic equilibrium equations at specific instants along the time axis. The typical problem to be solved is: knowing the configuration (geometrical configuration, velocities, accelerations, stresses, etc.) at time t seek for the configuration at time $t+\Delta t$ (Bathe, 1996).

Being $^{\tau}\underline{U}$ the vector of generalized nodal displacements (displacements and rotations) at a generic instant τ, the equilibrium equations at a time $t+\Delta t$ are:

$$\underline{M}\,^{t+\Delta t}\ddot{\underline{U}} + \underline{C}\,^{t+\Delta t}\dot{\underline{U}} = {}^{t+\Delta t}\underline{R} - {}^{t+\Delta t}\underline{F}. \tag{20}$$

In the above set of equations $\underline{M}$ is the mass matrix, $\underline{C}$ is the damping matrix, $^{t+\Delta t}\ddot{\underline{U}}$ is the vector of generalized nodal accelerations, $^{t+\Delta t}\dot{\underline{U}}$ is the vector of generalized nodal velocities, $^{t+\Delta t}\underline{R}$ is the vector of external generalized nodal loads and $^{t+\Delta t}\underline{F}$ is the

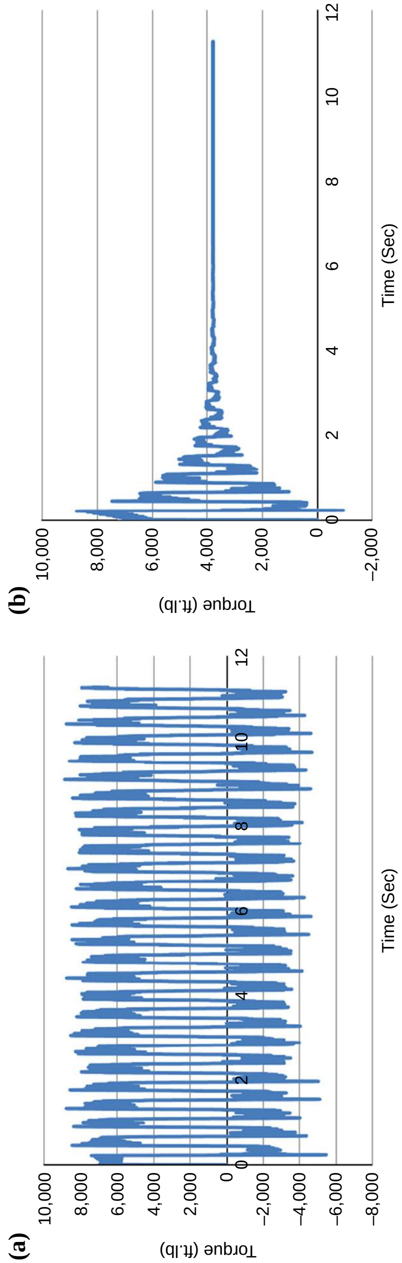

Figure 6.
Damping effect on torsional vibrations. (a) Result without considering the drilling mud damping; (b) result considering a drilling mud damping

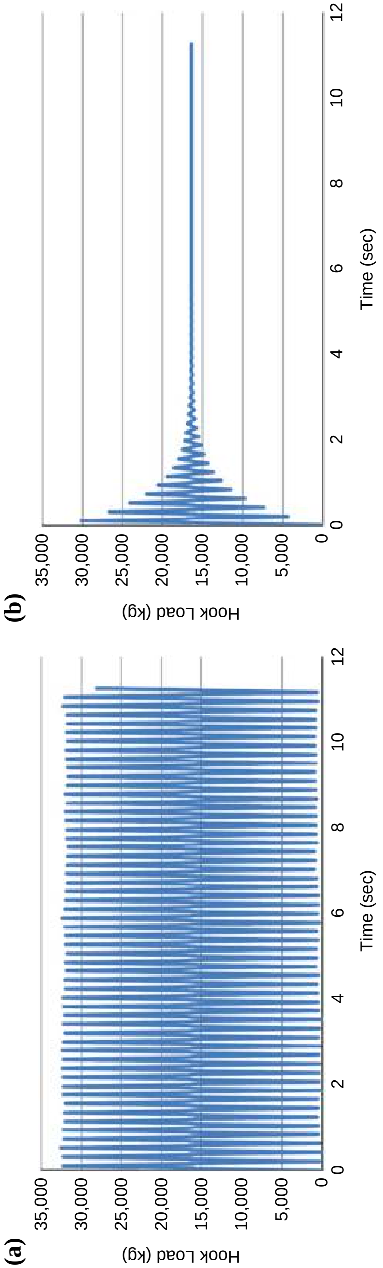

Figure 7.
Damping effect on axial vibrations. (a) Result without considering the drilling mud damping; (b) result considering a drilling mud damping

vector of generalized nodal internal forces; all of them at time $t+\Delta t$. The vector of internal forces is a function of the nodal generalized displacements; that is to say, ${}^{t+\Delta t}\underline{F} = {}^{t+\Delta t}\underline{F}\left({}^{t+\Delta t}\underline{U}\right)$.

We use an explicit time integration scheme (Wood, 1990):

$$ {}^{t+\Delta t}\underline{U} = {}^{t}\underline{U} + \Delta t\, {}^{t}\dot{\underline{U}} + \frac{1}{2}(\Delta t)^{2}\, {}^{t}\ddot{\underline{U}}; \tag{21} $$

$$ {}^{t+\Delta t}\dot{\underline{U}} = {}^{t}\dot{\underline{U}} + \frac{\Delta t}{2}\left({}^{t}\ddot{\underline{U}} + {}^{t+\Delta t}\ddot{\underline{U}}\right) \tag{22} $$

hence:

$$ \left(\underline{M} + \frac{\Delta t}{2}\underline{C}\right) {}^{t+\Delta t}\ddot{\underline{U}} = {}^{t+\Delta t}\underline{R} - {}^{t}\underline{F}\left({}^{t}\underline{U} + \Delta t\, {}^{t}\dot{\underline{U}} + \frac{1}{2}(\Delta t)^{2}\, {}^{t}\ddot{\underline{U}}\right) - \underline{C}\, {}^{t}\dot{\underline{U}} - \frac{\Delta t}{2}\underline{C}\, {}^{t}\ddot{\underline{U}}. \tag{23} $$

This explicit integration scheme is only stable if:

$$ \Delta t < \frac{T_{min}}{\pi} \tag{24} $$

where T_{min} is the minimum eigenperiod contained in the model (Bathe, 1996).

It is not practical to calculate all the eigenvalues of the system to determine the minimum eigenperiod and also, since the model is geometrically nonlinear, the value of T_{min} changes for each time step; hence, we will make a conservative heuristic approximation to determine Δt.

For each element *(e)* we calculate:

- $\Delta t_1^{(e)}$: the critical time step considering the bending of the isolated element under axial loading (A. R&D, 2012; Blevins, 1979);
- $\Delta t_2^{(e)}$: the critical time step considering the torsion of the isolated element (Blevins, 1979); and
- $\Delta t_3^{(e)}$: the critical time step considering the axial extension of the isolated element (Blevins, 1979).

Finally, based on our numerical experimentation we use for each time step:

$$ \Delta t = \alpha . min\left(\Delta t_1^{(e)}, \Delta t_2^{(e)}, \Delta t_3^{(e)}\right) \tag{25} $$

where $\alpha \leqslant 1$ (in our numerical experimentation we used $\alpha = 0.8$).

3. The simulation set-up

In this section we discuss the simulation set-up; that is to say, the main assumptions used to model the drilling processes, the required data input and the imposed boundary conditions.

3.1 Assumptions and data

3.1.1 The time intervals. A drilling process takes a given time for its completion. To analyze a complete process we subdivide it into intervals and assume that within each interval the process is stationary. Each process will be modeled using a "simulation window" (see Figure 8) (the simulation windows should be large enough to assure that a stationary behavior is achieved inside it).

3.1.2 The well geometry data. The target well geometry is introduced with the model pre-processor as discussed in Appendix and the pre-processor provides the simulator with a list of points defined by the (x, y, z) coordinates.

3.1.3 Drilling parameters data. For each "simulation window" characterizing a time interval, the user should specify the following data:

- number and type of pipes to be lowered in the well during the time interval;
- mud density and viscosity;
- required weight on the bit (WOB) (see Figure 9);
- Hook position (the load on the hook is a simulation result)[1];
- required torque on the bit (TOB) (see Figure 9);
- RPM of the bit;

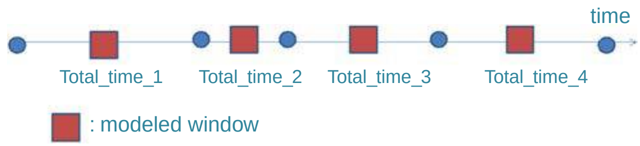

Figure 8. Time intervals in the middle of each time interval we indicate the simulation window

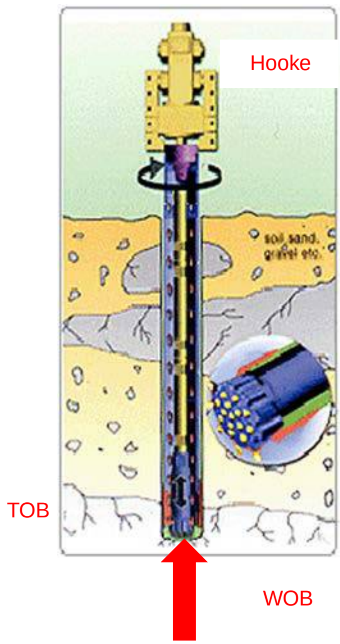

Figure 9. Schemeatic representation of TOB-WOB and Hook

- weight of the bottom hole assembly (BHA) which is the weight of the lower part of the drilling column containing the bit and the weights that are added in order to get a specified WOB;
- friction coefficient between the pipes and the well; and
- number of centralizers and their position[2].

3.2 Imposed boundary conditions

At the model first node the power tong RPM and the vertical position (hooke position) are imposed and at the model last node the formation reactions (WOB and TOB) are imposed along the axial direction of the last element (see Figure 9).

At each centralizer we impose a contact condition considering the small gap between the centralizers and the well.

4. Numerical example and model verification

In what follows we analyze a typical CWD case, the modeled well geometry is shown in Figure 10. DLS distribution in the modeled well (see Appendix).

In Table I we summarize the data corresponding to the analyzed case:

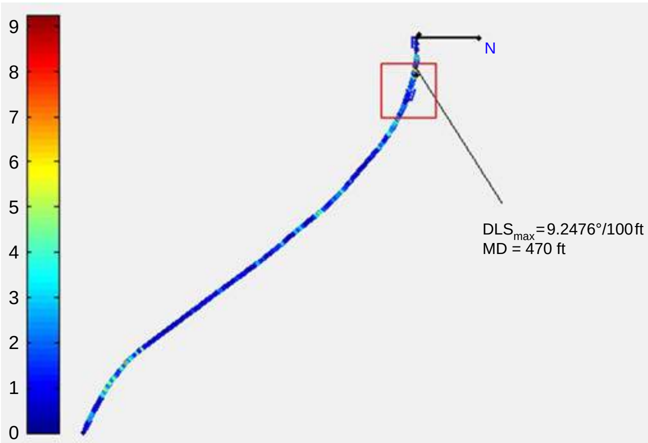

Figure 10. DLS distribution in the modeled well (see Appendix)

Table I. Data for the analyzed case

OD pipes (mm)	193.675
Thickness pipes (m)	9.525
OD boxes (mm)	215.900
Column length (m)	2,388.000
Number of pipes	199.000
RPM	80.000
Weight on the bit (WOB) (N)	0.000
Torque on the bit (TOB) (Nm)	1,514.334
Mud viscosity (cp)	10.000
Weight of BHA (N)	2,224.600
Friction coefficient pipes – formation	0.100

Considering individual pipes of 12 m of length, to verify the simulator results, we analyze the following cases (Table II).

The simulation starts with all the pipes in a vertical position (interfering with the well) and in the first time step the contact algorithm drives them inside the well; hence, the "simulation window" includes a transient response and converges to a stationary cyclic response.

In Figure 11 we show the relevant results for two of the analyzed cases.

The results provided by both sets of parameters are equivalent; however, NC = 10 gives a result with less spikes than NC = 2.

In Figures 12 and 13 we compare the results obtained with all the NC values.

In Figure 14 we present the calculated values for the hook load as a function of time.

The values of the time integration step (Equation (15)) are plotted in Figure 15.

5. Conclusions

With the purpose of providing a predictive tool for oil drilling engineers for the evaluation of wear and fatigue in drilling columns (especially when the casing while

Table II. Analysis parameters (see Section 2.2)

NC	2, 8, 9 and 10
Δt_c	0.0015 sec

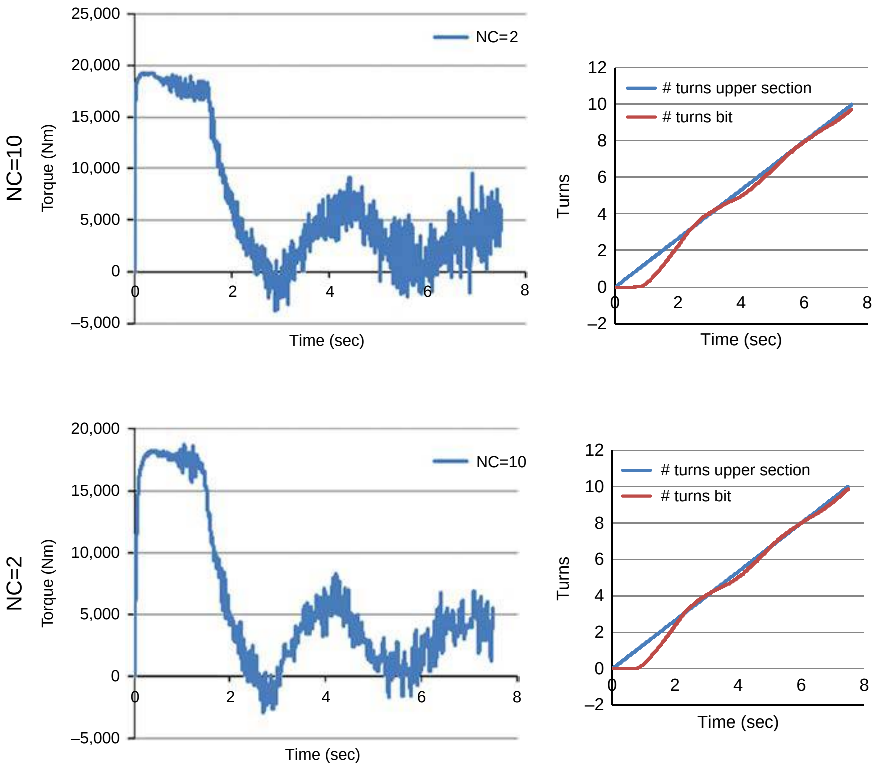

Figure 11. Simulation outputs

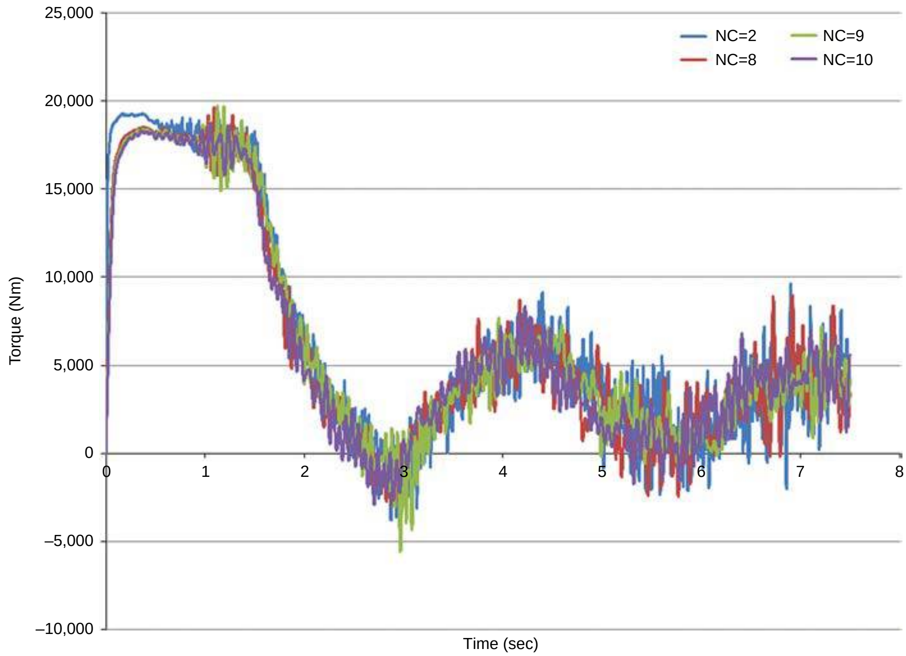

Figure 12. Complete set of results Torque – Time

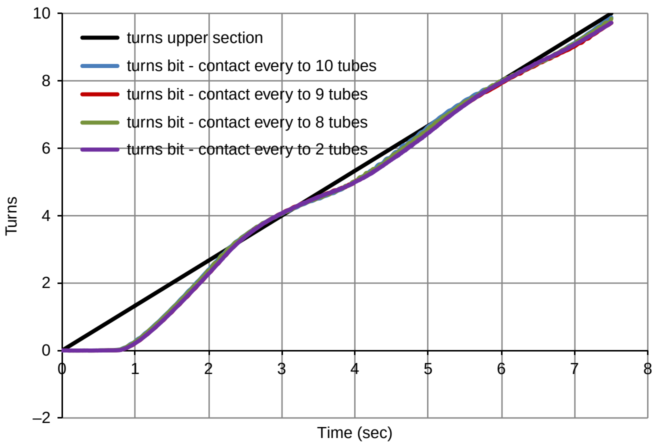

Figure 13. Complete set of results Turns – Time

drilling technique is used) a finite element code was developed for the simulation of the mechanical behavior of the pipe columns used in drilling processes.

The developed finite element simulator uses a co-rotational Bernoulli beam element, an explicit time integration scheme and an explicit contact algorithm.

The simulator incorporates the main variables that are used by drilling engineers in the definition of the drilling processes. The code is useful a priori, in the design of a drilling process, as a tool for comparing different designpp options and predicting their

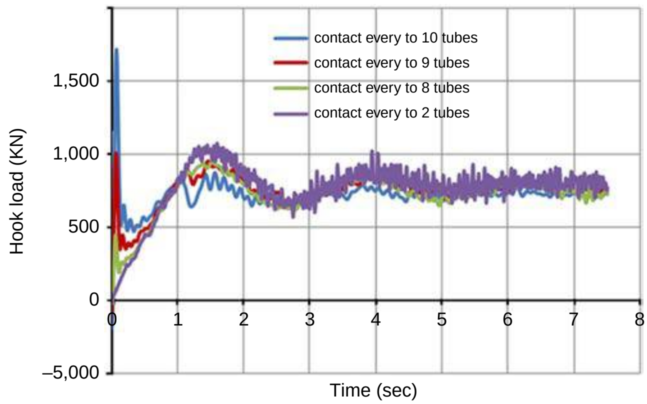

Figure 14.
Calculated hook load

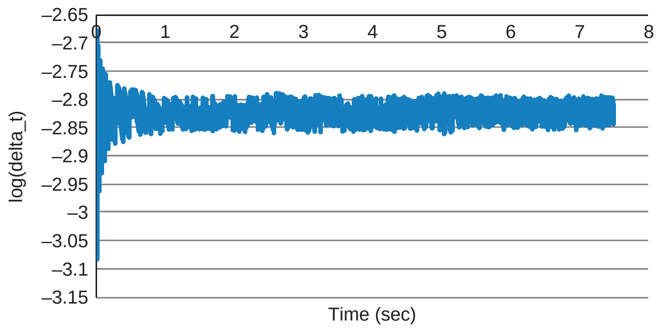

Figure 15.
Time integration steps

results and a posteriori of a failure to understand its genesis and therefore provide know-why to improve the drilling techniques.

The numerical results show that the simulator is stable and provides consistent solutions.

Notes

1. The drilling column hangs from a hook (see Figure 9).
2. The centralizers are disks mounted on the drilling column pipes whose outside diameters are close to the well and therefore have the task of centering the drilling column inside the well.

References

A. R&D (2012), *ADINA Users Manuial*, ADINA R&D, Watertown, MA.

Bathe, K.-J. (1996), *Finite Element Procedures*, Prentice Hall, Saddle River, NJ.

Bathe, K.-J. and Bolourchi, S. (1979), "Large displacement analysis of three-dimensional beam structures", *International Journal for Numerical Methods in Engineering*, Vol. 14 No. 7, pp. 961-986.

Blevins, R. (1979), *Formulas for Natural Frequency and Mode Shape*, Van Nostrand Reinhold Company, New York, NY.

Cirak, F. and West, M. (2005), "Decomposition contact response (DCR) for explicit finite element dynamics", *Int. J. Num. Methods Engng*, Vol. 64, pp. 1078-1110.

Dvorkin, E. and Goldschmit, M. (2005), *Nonlinear Continua*, Springer, Berlin.

Dvorkin, E. and Toscano, R. (2001), "Effects of internal/external pressure on the global buckling of pipelines", *De Proceedings of the First MIT Conference on Computational Fluid and Solid Mechanics*, *Cambridge, MA*.

Dvorkin, E., Oñate, E. and Oliver, J. (1988), "On a nonlinear formulation for curved Timoshenko beam elements considering large displacement/rotation increments", *Int. J. Numerical Methods in Engng*., Vol. 26, pp. 1597-1613.

Lubinski, A. and Althouse, W. (1962), "Helical buckling of tubing sealed in packers", *Journal of Petroleum Technology*, Vol. 97 No. 2, pp. 493-497.

Mitchell, R. (2003), "Lateral buckling of pipe with connectors in curved well bores", *SPE Drilling and Completion*, Vol. 18 No. 1, pp. 22-32.

Palmer, A. and Martin, J. (1975), "Buckle propagation in submarine pipelines", *Nature*, Vol. 254, pp. 46-48.

Rae, G., Lesso, W. and Sapijanskas, M. (2005), "Understanding torque and drag: best practices and lessons learnt from captain field's extended reach wells", *De SPE/IADC Drilling Conference*, *Amsterdam*.

Shathuvalli, U., Payne, M., Patillo, P. and Libesay, R. (2005), "Advanced assessment of drillpipe fatigue and application to critical well engineering", *De SPE/IADC Drilling Conference*, *Amsterdam*.

Sikal, A., Boulet, J., Menand, S. and Sellami, H. (2008), "Drillpipe stress distribution and cumulative fatigue analysis in complex wells drilling: new approach in fatigue optimization", *De SPE Annual Technical Conference and Exhibition*, *Denver, CO*.

Warren, T., Angman, P. and Houtchens, B. (2000), "Casing drilling application design considerations", *De IADC/SPE Drilling Conference*, *New Orleans, LA*.

Wood, W. (1990), *Practical Time-Stepping Schemes*, Clarendon Press, Oxford.

Further reading

Cunha, J.C. (2004), "Buckling of tubulars inside wellbores: a review on recent theoretical and experimental works", *SPE Drilling and Completion*, Vol. 19 No. 1, pp. 13-19.

Inglis, T. (1987), "Directional drilling", *De Petroleum Engineering and Development Studies*, Vol. 2, Grahan & Trotman.

Lubinski, A. (1950), "A study of the buckling of rotary drilling strings", *Drilling and Production Practice (API)*.

Mitchell, R.F. (1975), "The twist of a helical buckled casing", *Journal of Manufacturing Science and Engineering*, Vol. 97 No. 2, pp. 493-497.

Mitchell, R.F. (1982), "Buckling behavior of well tubing: the packer effect", *SPE Journal*, Vol. 22 No. 5, p. 616.

Mitchell, R.F. (1988), "New concepts for helical buckling", *SPE Drilling Engineering*, Vol. 3 No. 3, pp. 303-310.

Mitchell, R. (1995), "Pull-through forced in buckled tubing", *SPE Production & Facilities*, May.

Mitchell, R. (1996), "Comprehensive analysis of buckling with friction", *SPE Drilling and Completion*, September.

Mitchell, R. (1997), "Effects of well deviation on helical buckling", *SPE Drilling and Completion*, March.

Appendix. The well geometry

The well geometry is represented by the coordinates of position stations defined along the borehole axis. Using as parameters the usual ones (Azimuth, Inclination and Measured Depth) we get the representation indicated in Figure A1.

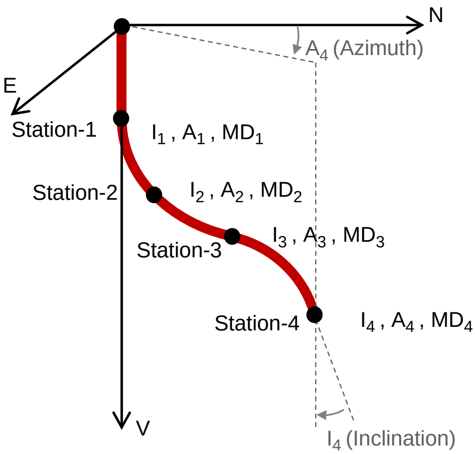

Figure A1.
Well outline

The Azimuth and Inclination angles are indicated in the figure; the measured depth (MD_k) is the distance along the well path between a survey station "k" and the reference level.

Knowing the Cartesian components of a station "$k-1$" we can calculate (with the angles measured in degrees):

$$\Delta\alpha_k = \cos^{-1}[\cos(I_{k-1})\cos(I_k) + \sin(I_{k-1})\sin(I_k)\cos(A_k - A_{k-1})]$$

$$RF_k = \left(\frac{180}{\pi}\right)\frac{2}{\Delta\alpha_k}\tan\left(\frac{\Delta\alpha_k}{2}\right)$$

$$V_k = V_{k-1} + \frac{\Delta MD_k}{2}[\cos(I_{k-1}) + \cos(I_k)]$$

$$N_k = N_{k-1} + \frac{\Delta MD_k}{2}[\sin(I_{k-1})\sin(A_{k-1}) + \sin(I_k)\sin(A_k)]\ \ RF_k$$

$$E_k = E_{k-1} + \frac{\Delta MD_k}{2}[\sin(I_{k-1})\cos(A_{k-1}) + \sin(I_k)\cos(A_k)]\ \ RF_k \qquad \text{(A1)}$$

The dog leg severity (DLS) at "K" is defined as:

$$DLS_k = \frac{100\ \ \Delta\alpha_k}{\Delta MD_k} \qquad \text{(A2)}$$

and the total vertical depth is:

$$If\ \ DLS_k = 0 \rightarrow \Delta TVD_k = \Delta MD_k\ \ \cos(I_k)$$

$$If\ \ DLS_k \neq 0 \rightarrow \Delta TVD_k = \frac{\Delta MD_k}{2}[\cos(I_{k-1}) + \cos(I_k)]\ \ RF_k \qquad \text{(A3)}$$

Corresponding author
Dr Eduardo Natalio Dvorki can be contacted at: edvorkin@simytec.com